Letter

Chiral terahertz lasing with Berry-curvature dipoles

Amin Hakimi,[1,*] Kasra Rouhi,[1,†] Tatiana G. Rappoport,[2,‡] Mário G. Silveirinha,[3,§] and Filippo Capolino[1,¶]

[1] *University of California, Irvine, Irvine, California 92697, USA*
[2] *Centro de Física das Universidade do Minho e do Porto, Universidade do Minho, Minho, Portugal*
[3] *Instituto Superior Técnico and Instituto de Telecomunicações, University of Lisbon, Avenida Rovisco Pais 1, 1049-001 Lisbon, Portugal*

(Received 21 January 2024; accepted 5 September 2024; published 16 October 2024)

Materials with Berry-curvature dipoles support a non-Hermitian electro-optic effect that is investigated here for lasing at terahertz frequencies. Such a system is conceived here as a stack of low-symmetry 2D materials. We show that a cavity made of such a material supports a nonreciprocal growing mode with elliptical polarization that generates an unstable resonance leading to self-sustained oscillations. Notably, we demonstrate that the chiral nature of the gain derived from the Berry dipole allows the manipulation of the laser light's handedness by a simple reversal of the electric field bias.

DOI: 10.1103/PhysRevApplied.22.L041003

Several optical and electronic phenomena are intricately connected to the geometry of electronic wave functions in solids, which is encoded in the Berry curvature [1]. Although generally associated with magnetic materials, the Berry curvature—which is odd under inversion symmetry—can be finite in momentum space in acentric nonmagnetic crystals [1]. Recent proposals suggest that electro-optic (EO) effects in this type of material can induce nonreciprocal optical *gain*, with the gain-dissipative response controlled by the light polarization and propagation direction [2–4]. This effect is rooted in the system's Berry-curvature dipole (BD) [5–7], the first moment of Berry curvature integrated over occupied states.

The BDs play a crucial role in various nonlinear electronic and optical effects. Notably, they enable a second-order nonlinear Hall effect without a magnetic field [8–10] and the rectifying of alternating current [11,12]. Materials with a BD can host a kinetic magnetoelectric effect, where an electric current generates a net magnetization [13–15]. The BD is also associated with optical phenomena, including the kinetic Faraday effect, where the rotatory power is proportional to the bias electric current and reverses sign with the bias [16–18], and the circular photogalvanic effect, where the photocurrent direction is locked to the helicity of the incoming light [6,19–21].

*Contact author: amin.hakimi@uci.edu
†Contact author: kasra.rouhi@uci.edu
‡Contact author: tgrappoport@fisica.uminho.pt
§Contact author: mario.silveirinha@tecnico.ulisboa.pt
¶Contact author: f.capolino@uci.edu

We present an investigation that underscores the potential application of the non-Hermitian linear EO effect in BD materials for terahertz lasing. We propose a mechanism for drawing energy from an appropriately biased BD material into a terahertz cavity. Notably, our laser exhibits nearly circular polarization, and due to the chiral characteristic of the Berry-dipole gain, the handedness of the emitted light is locked to the electric bias sign (Fig. 1). Our findings may be relevant for advancing terahertz and chiral-light technologies and offer valuable insights into potential applications of BD materials. Our theory builds on the total conductivity response of a generic low-symmetry 2D material derived in Ref. [3],

$$\underline{\boldsymbol{\sigma}}(\omega) = \frac{\sigma_0}{\gamma - i\omega}\begin{bmatrix} \omega_{\mathrm{F}} & \xi \\ 0 & \omega_{\mathrm{F}} \end{bmatrix} - \frac{\sigma_0}{\gamma}\begin{bmatrix} 0 & -\xi \\ \xi & 0 \end{bmatrix}, \quad (1)$$

where $\sigma_0 = 2e^2/h$ is the conductance quantum, $\gamma = 1/\tau$ is the scattering rate, and $\omega_{\mathrm{F}} = E_{\mathrm{F}}/\hbar$, where E_{F} is the Fermi level. The parameter ξ rules the linear EO response; it is proportional to the applied static electric field E_0 and to the BD of the material D_{B}: $\xi = \pi e D_{\mathrm{B}} E_0/\hbar$. Also, the EO response is valid for frequencies below the interband absorption threshold.

Without an electric bias ($\xi = 0$), the longitudinal optical conductivity is dominated by Drude's contribution $\sigma^{(1)}(\omega) = \sigma_{\mathrm{D}}(E_{\mathrm{F}})/(\gamma - i\omega)$, with $\sigma_{\mathrm{D}}(E_{\mathrm{F}}) = \sigma_0\omega_{\mathrm{F}}$. For simplicity, we ignore the anisotropic response of the 2D material so that $\sigma^{(1)}_{xx}(\omega) = \sigma^{(1)}_{yy}(\omega)$.

With a static bias, the optical response gets two additional components proportional to ξ: (i) a frequency-dependent term that can generate optical gain, in the first

 © 2024 American Physical Society

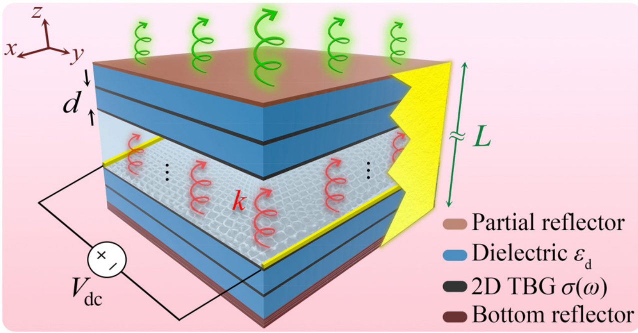

FIG. 1. Cavity made of a non-Hermitian material. The BDs are in the low-symmetry 2D materials, e.g., TBG, separated by a dielectric of thickness d. Terahertz radiation through the partial reflector at the top has either right or left handedness. The handedness of the top emission is flipped by reversal of the voltage bias.

matrix in Eq. (1), and (ii) a frequency-independent part that models a gyrotropic conservative response [second matrix in Eq. (1)]. The optical gain originates from non-Hermitian light-matter interactions mediated by the BD. A large BD is desirable to maximize these effects. In two dimensions, the BD components can be expressed in terms of contributions from states near the Fermi surface, $D_B^a = -\int (d^2k/(2\pi)^2)\Omega_{\mathbf{k}}(\partial f_{\mathbf{k}}^0/\partial k_a)$, where $\Omega_{\mathbf{k}}$ is the Berry curvature and $f_{\mathbf{k}}^0$ is the Fermi-Dirac distribution [5]. The BD depends on the product of the Berry curvature and the distribution function derivative. Thus, the most promising candidates for large BDs are systems with narrow gaps, such as those achieved through nanopatterning 2D materials [22] or in twisted bilayers [23–28]. These systems concentrate band velocity and Berry curvature near highly localized Dirac cones, enhancing the BD [23]. Very large BDs have also been observed in oxide interfaces [29,30].

Here we assume that the non-Hermitian material is composed of a stack of low-symmetry 2D materials with a large BD that are modeled by Dirac-like Hamiltonians. As an example, we consider twisted bilayer graphene (TBG) layers. The layers are biased by a dc electric field along the y direction that induces a drift current. The BDs provide the mechanism to transfer energy from drifting electrons to the terahertz field [3]. These non-Hermitian interactions are controlled by the handedness of the terahertz field. Each dielectric spacer has subwavelength thickness d and relative permittivity $\varepsilon_d = \varepsilon_d' + i\varepsilon_d''$. The 2D-material layers are isolated from their neighbors, so their electronic responses are independent.

For simplicity, following the analysis in Ref. [31] for a stack of isotropic graphene layers, we construct an equivalent homogeneous anisotropic medium with effective relative permittivity $\underline{\boldsymbol{\varepsilon}} = \underline{\boldsymbol{\varepsilon}}_t + \varepsilon_z\hat{\mathbf{z}}\hat{\mathbf{z}}$ (see Supplemental Material [32]). As the 2D material is infinitesimally thin compared with the thickness of the dielectric spacer, the longitudinal permittivity is expressed simply as $\varepsilon_z = \varepsilon_d$, whereas the transverse effective relative permittivity dyad takes the form $\underline{\boldsymbol{\varepsilon}}_t = \varepsilon_d\underline{\mathbf{I}} + i\underline{\boldsymbol{\sigma}}/(\omega\varepsilon_0 d)$, where $\underline{\mathbf{I}}$ is the identity dyad.

We focus on wave propagation along the z direction of homogenized (i.e., spatially averaged) fields $\mathbf{E} \propto e^{ikz}$, with $\mathbf{E}$ confined in the transverse plane. Hence, we consider the dyad $\underline{\boldsymbol{\varepsilon}}_t$, which is written in matrix form as

$$\underline{\boldsymbol{\varepsilon}}_t = \begin{bmatrix} \varepsilon_a & \varepsilon_b \\ \varepsilon_c & \varepsilon_a \end{bmatrix}, \qquad (2)$$

where the elements of the non-Hermitian matrix are $\varepsilon_a = \varepsilon_d + i\omega_0\omega_F/(\omega(\gamma - i\omega))$, $\varepsilon_b = i(\omega_0/\omega)\xi(1/(\gamma - i\omega) + 1/\gamma)$, and $\varepsilon_c = -i\omega_0\xi/(\omega\gamma)$, and $\omega_0 = \sigma_0/(\varepsilon_0 d)$. The eigenvalues of $\underline{\boldsymbol{\varepsilon}}_t$ are $\varepsilon_{1,2} = \varepsilon_a \pm \sqrt{\varepsilon_b\varepsilon_c}$, and the corresponding two polarization eigenvectors are $\mathbf{E}_{1,2} = \left[\pm\sqrt{\varepsilon_b/\varepsilon_c}, 1\right]^T$ (T is the transpose operator). They are rewritten in terms of the TBG parameters as

$$\varepsilon_{1,2} = \varepsilon_d + \frac{\omega_0}{\omega}\left(\frac{-\frac{\omega_F}{\omega}}{1 + i\frac{\gamma}{\omega}} \pm \frac{\xi}{\gamma}\sqrt{\frac{1 + 2i\frac{\gamma}{\omega}}{1 + i\frac{\gamma}{\omega}}}\right), \qquad (3a)$$

$$\mathbf{E}_{1,2} = \begin{bmatrix} i\sqrt{\frac{1+i2\gamma/\omega}{1+i\gamma/\omega}} \\ 1 \end{bmatrix}, \begin{bmatrix} -i\sqrt{\frac{1+i2\gamma/\omega}{1+i\gamma/\omega}} \\ 1 \end{bmatrix}. \qquad (3b)$$

The eigenvalue ε_2 may have $\mathrm{Im}(\varepsilon_2) < 0$, providing a medium with gain. While it is well known that Berry curvature can affect the current due to optical bias, this current does not inherently result in optical gain. Indeed, the standard Hall effect does not entail either gain or dissipation. Therefore, the non-Hermitian EO effect discussed here is a quite unique mechanism that mimics the functionality of a transistor within bulk material. While the eigenvalues depend on ω_F and ξ, the two elliptical polarization eigenvectors depend only on γ and ω; in other words, the gain parameter ξ has no effect on the polarization of the eigenstates. Furthermore, the two eigenvectors in Eq. (3b) are also eigenvectors of the conductivity matrix in Eq. (1). Therefore, the polarization eigenstates of TBG are the same as those of the homogenized material described by the effective permittivity. Because of the non-Hermiticity of the permittivity, the two polarization eigenstates are not orthogonal, and are represented in Fig. 2 at three different frequencies, assuming that $\gamma = 10^{12}$ s^{-1}. They tend to be orthogonal with circular polarization when $\omega \gg \gamma$.

At high frequencies (i.e., when $\omega/\gamma \gg 1$ and $\omega/\gamma \gg \omega_F/\xi$), the eigenvalues are simplified as $\varepsilon_{1,2} \approx \varepsilon_d \pm \omega_0\xi/(\omega\gamma)$. Since the term $\omega_0|\xi|/(\omega\gamma)$ can be larger than ε_d, $\mathrm{Re}(\varepsilon_1)$ and $\mathrm{Re}(\varepsilon_2)$ can be either positive or negative, whereas for sufficiently large frequencies, both $\mathrm{Re}(\varepsilon_1)$ and $\mathrm{Re}(\varepsilon_2)$ tend to be positive.

A wave propagating along the z direction in the homogenized anisotropic medium is governed by the wave equation $k_0^2\,\underline{\boldsymbol{\varepsilon}}_t \cdot \mathbf{E} - k^2\mathbf{E} = 0$, where $k_0 = \omega\sqrt{\mu_0\varepsilon_0}$ is the

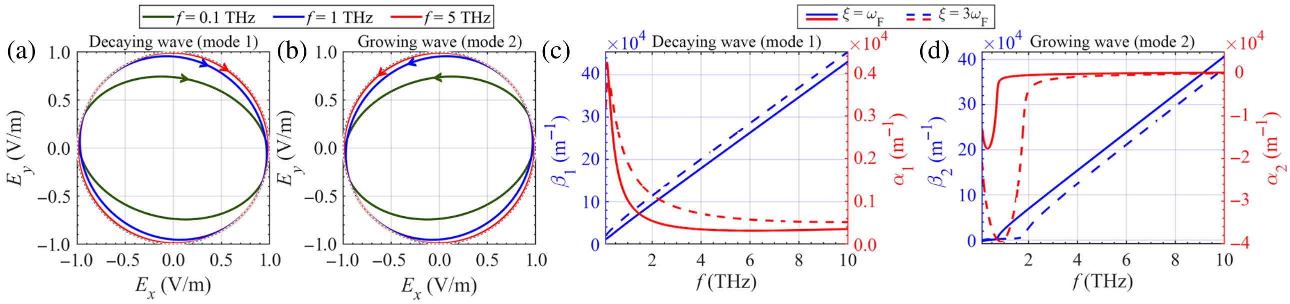

FIG. 2. (a),(b) Polarization curves and handedness for the (a) decaying and (b) growing waves at three different frequencies. (c),(d) Real (β_i) and imaginary (α_i) parts of the complex wavenumbers: (c) k_1 (decaying wave) and (d) k_2 (growing wave) with gain parameter $\xi = \omega_F$ (solid lines) and $\xi = 3\omega_F$ (dashed lines) by varying frequency.

free-space wavenumber (see Supplemental Material [32]). The eigenvalues k^2 are expressed in terms of the eigenvalues of $\underline{\boldsymbol{\varepsilon}}_t$ as $k_1^2 = k_0^2\varepsilon_1$ and $k_2^2 = k_0^2\varepsilon_2$, leading to $k_i = k_0\sqrt{\varepsilon_a \pm \sqrt{\varepsilon_b\varepsilon_c}}$, with $i = 1, 2$. As both k and $-k$ are solutions, in the following we focus only on the two solutions with a positive $\beta_i = \mathrm{Re}(k_i)$, with $\alpha_i = \mathrm{Im}(k_i)$ representing either the attenuation constant ($i = 1$) or the amplification constant ($i = 2$) of each mode. The nonorthogonal-polarization eigenstates $i = 1, 2$ correspond to the two eigenvectors of the non-Hermitian matrix $\underline{\boldsymbol{\varepsilon}}_t$. The two wavenumbers are expressed in terms of the TBG parameters as

$$k_i = k_0\sqrt{\varepsilon_d + \frac{\omega_0}{\omega}\left(\frac{-\frac{\omega_F}{\omega}}{1+i\frac{\gamma}{\omega}} \pm \frac{\xi}{\gamma}\sqrt{\frac{1+2i\frac{\gamma}{\omega}}{1+i\frac{\gamma}{\omega}}}\right)}. \quad (4)$$

Figure 2 shows the wavenumbers, for a material made of a stack of TBG with, the same as in Ref. [3], $\gamma = 10^{12}$ s^{-1}, $\omega_F/(2\pi) = 0.24$ THz, and a dielectric spacer with $\varepsilon_d' = 4$, $\varepsilon_d'' = 5 \times 10^{-3}$, and $d = 900$ nm, when $\xi = \omega_F$ (solid lines) and $\xi = 3\omega_F$ (dashed lines) are used. These are the default parameters used in all simulations. The level of optical gain is consistent with the numerical calculation of the BD of TBG for an electric field on the order of 0.1 V/μm and a BD on the order of $D_B = 10$ nm [3]. However, the same approach is valid for any 2D material modeled by a tilted Dirac Hamiltonian. As we can see in Fig. 2(d), the imaginary part of k_2 is negative, while the real part is positive. Therefore, for positive ξ, mode 2 grows exponentially along the z direction when $\alpha_2 < 0$, and mode 1 decays exponentially ($\alpha_1 > 0$).

If one inverts the polarization bias V_{dc}, i.e., the direction of the drift current, ξ changes sign [3], and the polarization $\mathbf{E}_1$ is the one subject to gain. Thus, unlike conventional lasers, which necessitate a stabilization mechanism to regulate the polarization of emitted light—often using methods such as the insertion of polarizers within the optical cavity to enforce linear polarization—our system allows the control of light handedness simply by alteration of the direction of the dc bias. Thereby, differently from conventional gain systems, a BD material with $\xi > 0$ provides gain only when the field polarization has a very specific handedness determined by $\mathbf{E}_2$. The fact that mode 2 is amplifying is verified by the expression for the Poynting vector along the z direction, $\mathrm{Re}(S_{z2}) = (\beta_2/(2\omega\mu_0))|\mathbf{E}_2|^2 > 0$, which confirms the positive power flow in the $+z$ direction while growing exponentially. Note that the wave with wavenumber $-k_2$, also associated with the polarization state $\mathbf{E}_2$, amplifies along the $-z$ direction because of chirality of the light propagating in the structure. It is remarkable that since mode 2 is polarized as $\mathbf{E}_2$ for wavenumbers k_2 and $-k_2$ the system is nonreciprocal because the two modes with k_2 and $-k_2$ have opposite handedness with respect to the propagation direction. Therefore, we have demonstrated that the non-Hermitian EO effect leads to the amplification of mode 2 in both directions and to the attenuation of mode 1 when $\xi > 0$. This enables the possibility to have a cavity with a convectional instability relying only on mode 2, leading to lasing. By reversal of the bias, the lasing action would be determined by the polarization $\mathbf{E}_1$, allowing the laser to radiate a desired handedness by one just controlling the biasing-voltage V_{dc} direction. Under the assumption that $\omega \gg \gamma$, the wavenumber of the amplifying mode in Eq. (4) is approximated as

$$k_2 \approx k_0\sqrt{\varepsilon_d - \frac{\omega_0\xi}{\omega\gamma} - \frac{\omega_0}{\omega^2}\left(\omega_F + i\frac{\xi}{2}\right)}. \quad (5)$$

There are two gain regimes. The first one is the "small-gain regime," when $\varepsilon_d' > \omega_0\xi/(\omega\gamma)$, leading to the wavenumber in Eq. (5) being mainly real, approximated as

$$\frac{\beta_2}{k_0} \approx \sqrt{\varepsilon_d' - \frac{\omega_0\xi}{\omega\gamma}}, \qquad \frac{\alpha_2}{k_0} \approx -\frac{\frac{\omega_0\xi}{2\omega^2} - \varepsilon_d''}{2\sqrt{\varepsilon_d' - \frac{\omega_0\xi}{\omega\gamma}}}. \quad (6)$$

The sign of α_2 is negative as long as $\omega_0\xi/(2\omega^2) > \varepsilon_d''$, and it becomes positive at large-enough frequencies.

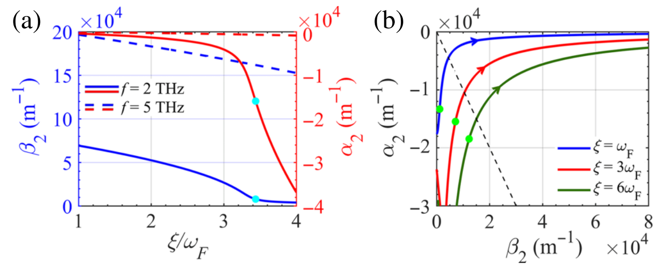

FIG. 3. (a) Real and imaginary parts of k_2 (amplifying wave) [Eq. (4)] as a function of gain. The light-blue dots show when $\xi = \xi_c$. The focus is on the small-gain regime. (b) Complex k_2 with frequency variation, showing the low-gain and high-gain regimes. The dashed black line is the bisector of the fourth quadrant. Green dots show when $\omega = \omega_c$.

Instead, under the "high-gain regime" $\omega_0\xi/(\omega\gamma) > \varepsilon'_d$, the wavenumber in Eq. (5) reduces to

$$\frac{\beta_2}{k_0} \approx \frac{\frac{\omega_0\xi}{2\omega^2} - \varepsilon''_d}{2\sqrt{\frac{\omega_0\xi}{\omega\gamma} - \varepsilon'_d}}, \qquad \frac{\alpha_2}{k_0} \approx -\sqrt{\frac{\omega_0\xi}{\omega\gamma} - \varepsilon'_d}. \tag{7}$$

This latter high-gain regime condition leads to a large convective amplification rate of mode 2. The two gain regimes show swapped expressions for α_2 and β_2; they are separated by the condition $\varepsilon'_d = \omega_0\xi/(\omega\gamma)$, which leads to the defining of a "critical gain" given by $\xi_c \approx \omega(\varepsilon'_d\gamma/\omega_0)$ and a "critical frequency" as $\omega_c = \omega_0\xi/(\varepsilon'_d\gamma)$ that represents the transition between these two gain regimes [see the blue and green dots in Figs. 3(a) and 3(b)]. Establishing a lasing condition within the small-gain regime ($\xi < \xi_c$) may also present some advantages due to its larger β_2.

The volume power density delivered to the EO material is given by $p_v \approx (\omega\varepsilon_0/2)\left[\varepsilon''_{xx}|\mathbf{E}|^2 + \omega_0\omega^{-2}\xi\,\mathrm{Im}\left(E_x E_y^*\right)\right]$, as shown in Supplemental Material [32]. Gain occurs when $p_v < 0$. The formula shows that (i) a degree of circular polarization is required to provide a negative value, and (ii) the presence of the BD D_B is responsible for providing both the gain value ξ and the elliptical polarization of the eigenmodes to make $\mathrm{Im}\left(E_x E_y^*\right) < 0$.

A laser operating at terahertz frequencies is conceived by enclosing the material with BDs in a cavity made of two mirrors separated by distance L, as in Fig. 1. The growing wave (mode 2) creates self-sustained oscillations, with power emitted from the top surface. We consider only mode 2 propagating within the cavity since mode 1 is attenuating and planar mirrors do not depolarize mode 2. The threshold gain and phase condition for such a self-sustained mechanism is given by

$$Re^{-2\alpha_2 L}e^{i(2\beta_2 L - \phi)} = -1, \tag{8}$$

where R and ϕ are the magnitude and phase of the electric field reflection coefficient at the top partial reflector. For

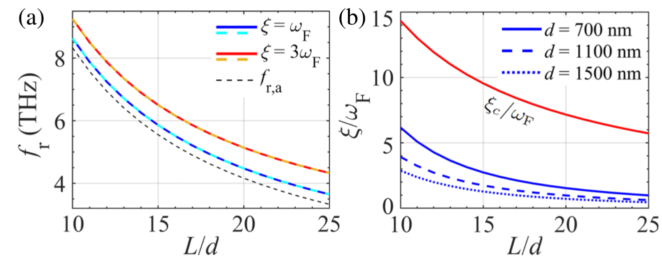

FIG. 4. (a) Oscillation frequency f_r versus L/d. Solid blue and red curves are solutions of Eq. (9), and dashed orange and light-blue curves are $\mathrm{Re}(\omega/(2\pi))$ from the approximated solution in Eq. (10). The dashed black curve shows the approximate $f_{r,a} \approx c/(2L\sqrt{\varepsilon'_d})$. (b) Normalized threshold gain ξ_{th}/ω_F for $R = 0.99$ versus L/d for different layer thicknesses d. In all three cases, the threshold gain is in the small-gain regime $\xi_{th} < \xi_c$.

simplicity, we assume that the bottom mirror is a perfect electric conductor providing a reflection coefficient of -1. Furthermore, without loss of generality, we take $\phi = \pi$. Then, the first fundamental oscillation frequency is given by the resonant condition

$$\beta_2(f) = \pi/L. \tag{9}$$

The cavity resonance f_r [solution of Eq. (9)] is provided in Fig. 4(a) (solid curves). With use of the approximate solution in Eq. (5), a closed-form expression for the first cavity angular eigenfrequency that satisfies Eq. (8) is

$$\omega \approx \frac{\omega_0\xi}{2\varepsilon_d\gamma} + \sqrt{\left(\frac{\omega_0\xi}{2\varepsilon_d\gamma}\right)^2 + \frac{\omega_0}{\varepsilon_d}\left(\omega_F + i\frac{\xi}{2}\right) + \frac{c^2}{\varepsilon_d}A^2}, \tag{10}$$

where $A = (1/(2L))\,(i\ln R + 2\pi)$. The real part of this natural frequency is plotted in Fig. 4(a) (dashed blue and orange curves), superimposed on the exact solution obtained from Eq. (9) (solid lines). Figure 4(a) also presents $f_{r,a} \approx c/(2L\sqrt{\varepsilon'_d})$ (dashed black curve), which is obtained by one combining Eqs. (6) and (9).

From Eq. (8), a necessary condition for establishing oscillations is that $\alpha_2 < \alpha_{th}$, with $\alpha_{th} = (1/(2L))\ln(R)$ (i.e., $|\alpha_2| > |\alpha_{th}|$, since $\alpha_{th} < 0$ due to $R < 1$). An estimate is derived by use of the approximation in Eq. (6), assuming that $\omega_0\xi/(\omega\gamma) \ll \varepsilon'_d$, leading to $\alpha_2 \approx -\xi\omega_0\beta_2/(4\varepsilon'_d\omega^2)$. This approximation, together with Eq. (9), leads to the threshold-gain condition

$$\xi_{th} \approx -\ln(R)\frac{2\pi c^2}{\omega_0}\frac{1}{L^2}. \tag{11}$$

The instability of the electromagnetic field within the cavity manifests itself at the onset of the lasing condition, and it can also be discerned by one observing the sign of $\mathrm{Im}(\omega)$. According to Eq. (10), one has $\mathrm{Im}(\omega) > 0$ when $\xi > \xi_{th}$.

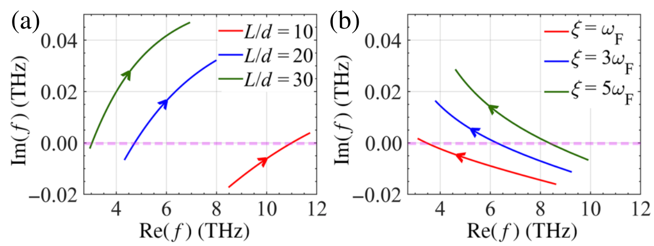

FIG. 5. Imaginary part versus real part of the laser natural frequency [Eq. (10)] with variation of (a) ξ ($0.5 < \xi/\omega_F < 10$) and (b) L ($10 < L/d < 30$). Lasing arises when $\mathrm{Im}(f) > 0$. For operation slightly above the threshold, the lasing frequency is roughly $\mathrm{Re}(f)$ at $\mathrm{Im}(f) = 0$, which is in the terahertz region.

We determine the scaling laws for the oscillation frequency $f_r \propto 1/L$ and threshold gain $\xi_{th} \propto 1/L^2$ from Eqs. (9) and (11). Furthermore, insertion of the estimate of the oscillation frequency $f_{r,a}$ into the "critical gain" expression leads to the trend $\xi_c \approx (\pi c\sqrt{\varepsilon_d'}\gamma/\omega_0)(1/L)$. Therefore, because of the scaling laws $\xi_{th} \propto 1/L^2$ and $\xi_c \propto 1/L$, by increasing the cavity length it is possible to have a threshold gain in the small-gain regime. The normalized threshold gain ξ_{th} from Eq. (11) is shown in Fig. 4(b) for variation of L/d; the plot confirms that operation above the threshold is possible, leading to lasing under the small-gain regime $\xi_{th} < \xi < \xi_c$. The normalized threshold gain ξ_{th}/ω_F ranges from 1 to 4 for $d > 800$ nm. Furthermore, Fig. 5 shows that it is possible to have gain above the threshold at a lasing frequency in the range from 3 to 12 THz. Any point above the horizontal dashed pink line indicates a cavity signal growing in time (i.e., above the threshold). The intersections with the dashed pink line represent the threshold [marginally stable field solution with $\mathrm{Im}(f) = 0$], showing also the estimate of the lasing frequency $\mathrm{Re}(f)$. For example, a gain parameter ξ as low as ω_F can induce lasing oscillations at 3.4 THz for $L/d \approx 27$.

In conclusion, we have introduced a perspective for terahertz lasing, leveraging the non-Hermitian linear EO effect in materials with Berry curvature. The distinctive feature of our approach lies in the chiral nature of the Berry-dipole gain, imparting a well-defined handedness to the laser fields. This characteristic can be easily adjusted by inversion of the static electric bias. Our solution holds great promise for a myriad of applications, offering versatility and adaptability in the realm of terahertz technology.

Acknowledgements. M.G.S. acknowledges the Institution of Engineering and Technology, the Simons Foundation (Award No. 733700), and Fundação para a Ciência e a Tecnologia and Instituto de Telecomunicações under Project No. UIDB/50008/2020. T.G.R. acknowledges funding from Fundação para a Ciência e a Tecnologia through Grant No. CEECIND/07471/2022

[1] D. Xiao, M.-C. Chang, and Q. Niu, Berry phase effects on electronic properties, Rev. Mod. Phys. **82**, 1959 (2010).

[2] S. Lannebère, D. E. Fernandes, T. A. Morgado, and M. G. Silveirinha, Nonreciprocal and non-Hermitian material response inspired by semiconductor transistors, Phys. Rev. Lett. **128**, 013902 (2022).

[3] T. G. Rappoport, T. A. Morgado, S. Lannebère, and M. G. Silveirinha, Engineering transistorlike optical gain in two-dimensional materials with Berry curvature dipoles, Phys. Rev. Lett. **130**, 076901 (2023).

[4] L.-K. Shi, O. Matsyshyn, J. C. W. Song, and I. S. Villadiego, Berry-dipole photovoltaic demon and the thermodynamics of photocurrent generation within the optical gap of metals, Phys. Rev. B **107**, 125151 (2023).

[5] I. Sodemann and L. Fu, Quantum nonlinear Hall effect induced by Berry curvature dipole in time-reversal invariant materials, Phys. Rev. Lett. **115**, 216806 (2015).

[6] S.-Y. Xu, Q. Ma, H. Shen, V. Fatemi, S. Wu, T.-R. Chang, G. Chang, A. M. M. Valdivia, C.-K. Chan, Q. D. Gibson *et al.*, Electrically switchable Berry curvature dipole in the monolayer topological insulator WTe_2, Nat. Phys. **14**, 900 (2018).

[7] Y. Zhang and L. Fu, Terahertz detection based on nonlinear Hall effect without magnetic field, Proc. Natl. Acad. Sci. **118**, e2100736118 (2021).

[8] Q. Ma, S.-Y. Xu, H. Shen, D. MacNeill, V. Fatemi, T.-R. Chang, A. M. Mier Valdivia, S. Wu, Z. Du, C.-H. Hsu *et al.*, Observation of the nonlinear Hall effect under time-reversal-symmetric conditions, Nature **565**, 337 (2019).

[9] K. Kang, T. Li, E. Sohn, J. Shan, and K. F. Mak, Nonlinear anomalous Hall effect in few-layer WTe_2, Nat. Mater. **18**, 324 (2019).

[10] Z. Du, H.-Z. Lu, and X. Xie, Nonlinear Hall effects, Nat. Rev. Phys. **3**, 744 (2021).

[11] D. Kumar, C.-H. Hsu, R. Sharma, T.-R. Chang, P. Yu, J. Wang, G. Eda, G. Liang, and H. Yang, Room-temperature nonlinear Hall effect and wireless radiofrequency rectification in Weyl semimetal $TaIrTe_4$, Nat. Nanotechnol. **16**, 421 (2021).

[12] L. Min, H. Tan, Z. Xie, L. Miao, R. Zhang, S. H. Lee, V. Gopalan, C.-X. Liu, N. Alem, B. Yan *et al.*, Strong room-temperature bulk nonlinear Hall effect in a spin-valley locked Dirac material, Nat. Commun. **14**, 364 (2023).

[13] V. Shalygin, A. Sofronov, L. Vorob'ev, and I. Farbshtein, Current-induced spin polarization of holes in tellurium, Phys. Solid State **54**, 2362 (2012).

[14] T. Furukawa, Y. Shimokawa, K. Kobayashi, and T. Itou, Observation of current-induced bulk magnetization in elemental tellurium, Nat. Commun. **8**, 954 (2017).

[15] F. Calavalle, M. Suárez-Rodríguez, B. Martín-García, A. Johansson, D. C. Vaz, H. Yang, I. V. Maznichenko, S. Ostanin, A. Mateo-Alonso, A. Chuvilin *et al.*, Gate-tuneable and chirality-dependent charge-to-spin conversion in tellurium nanowires, Nat. Mater. **21**, 526 (2022).

[16] E. L. Vorob'ev, E. L. Ivchenko, G. E. Pikus, I. I. Farbshtein, V. A. Shalygin, and A. V. Shturbin, Optical activity in tellurium induced by a current, J. Exp. Theor. Phys. Lett. **29**, 441 (1979).

[17] S. S. Tsirkin, P. A. Puente, and I. Souza, Gyrotropic effects in trigonal tellurium studied from first principles, Phys. Rev. B **97**, 035158 (2018).

[18] E. J. König, M. Dzero, A. Levchenko, and D. A. Pesin, Gyrotropic Hall effect in Berry-curved materials, Phys. Rev. B **99**, 155404 (2019).

[19] E. L. Ivchenko and G. E. Pikus, New photogalvanic effect in gyrotropic crystals, J. Exp. Theor. Phys. Lett. **27**, 604 (1978).

[20] V. M. Asnin, A. A. Bakun, A. M. Danishevskii, E. L. Ivchenko, G. E. Pikus, and A. A. Rogachev, Observation of a photo-emf that depends on the sign of the circular polarization of the light, J. Exp. Theor. Phys. Lett. **28**, 74 (1978).

[21] E. Deyo, L. Golub, E. Ivchenko, and B. Spivak, Semi-classical theory of the photogalvanic effect in non-centrosymmetric systems, arXiv preprint arXiv:0904.1917.

[22] S.-C. Ho, C.-H. Chang, Y.-C. Hsieh, S.-T. Lo, B. Huang, T.-H.-Y. Vu, C. Ortix, and T.-M. Chen, Hall effects in artificially corrugated bilayer graphene without breaking time-reversal symmetry, Nat. Electron. **4**, 116 (2021).

[23] Z. He and H. Weng, Giant nonlinear Hall effect in twisted bilayer WTe_2, npj Quantum Mater. **6**, 101 (2021).

[24] P. A. Pantaleón, T. Low, and F. Guinea, Tunable large Berry dipole in strained twisted bilayer graphene, Phys. Rev. B **103**, 205403 (2021).

[25] J. Duan, Y. Jian, Y. Gao, H. Peng, J. Zhong, Q. Feng, J. Mao, and Y. Yao, Giant second-order nonlinear Hall effect in twisted bilayer graphene, Phys. Rev. Lett. **129**, 186801 (2022).

[26] S. Sinha, P. C. Adak, A. Chakraborty, K. Das, K. Debnath, L. V. Sangani, K. Watanabe, T. Taniguchi, U. V. Waghmare, A. Agarwal *et al.*, Berry curvature dipole senses topological transition in a moiré superlattice, Nat. Phys. **18**, 765 (2022).

[27] K. Kang, W. Zhao, Y. Zeng, K. Watanabe, T. Taniguchi, J. Shan, and K. F. Mak, Switchable moiré potentials in ferroelectric WTe_2/WSe_2 superlattices, Nat. Nanotechnol. **18**, 861 (2023).

[28] M. Huang, Z. Wu, X. Zhang, X. Feng, Z. Zhou, S. Wang, Y. Chen, C. Cheng, K. Sun, Z. Y. Meng *et al.*, Intrinsic nonlinear Hall effect and gate-switchable Berry curvature sliding in twisted bilayer graphene, Phys. Rev. Lett. **131**, 066301 (2023).

[29] E. Lesne, Y. G. Sağlam, R. Battilomo, M. T. Mercaldo, T. C. van Thiel, U. Filippozzi, C. Noce, M. Cuoco, G. A. Steele, C. Ortix *et al.*, Designing spin and orbital sources of Berry curvature at oxide interfaces, Nat. Mater. **22**, 576 (2023).

[30] M. T. Mercaldo, C. Noce, A. D. Caviglia, M. Cuoco, and C. Ortix, Orbital design of Berry curvature: Pinch points and giant dipoles induced by crystal fields, npj Quantum Mater. **8**, 12 (2023).

[31] M. A. Othman, C. Guclu, and F. Capolino, Graphene-based tunable hyperbolic metamaterials and enhanced near-field absorption, Opt. Express **21**, 7614 (2013).

[32] See Supplemental Material at http://link.aps.org/supplemental/10.1103/PhysRevApplied.22.L041003 for (1) the linear electro-optic response, (2) the effective-medium approximation, (3) wave propagation in a homogenized anisotropic medium, (4) power transfer from the EO material to the terahertz wave, (5) the coalescence parameter and nonorthogonality of the eigenmodes, and (6) threshold-gain analysis, in which Refs. [3,24,31,33–37] are cited.

[33] R. Bistritzer and A. H. MacDonald, Moiré bands in twisted double-layer graphene, Proc. Natl. Acad. Sci. **108**, 12233 (2011).

[34] G. Franceschetti, *Campi Elettromagnetici* (Bollati Boringhieri, Turin, Italy, 1988), 2nd ed., Chap. 1.

[35] L. B. Felsen and N. Marcuvitz, *Radiation and Scattering of Waves* (Prentice-Hall, Englewood Cliffs, NJ, 1973), p. 79.

[36] A. F. Abdelshafy, M. A. Othman, D. Oshmarin, A. T. Almutawa, and F. Capolino, Exceptional points of degeneracy in periodic coupled waveguides and the interplay of gain and radiation loss: Theoretical and experimental demonstration, IEEE Trans. Antennas Propag. **67**, 6909 (2019).

[37] M. Y. Nada, T. Mealy, and F. Capolino, Frozen mode in three-way periodic microstrip coupled waveguide, IEEE Microw. Wirel. Compon. Lett. **31**, 229 (2020).